Bias of the Steady-State Averaged Solutions of a Strongly Overdamped Particle in a Cosine Potential Under Harmonic Excitation

Attila Genda[1], Alexander Fidlin[1], and Oleg Gendelman[2]

[1] Karlsruhe Institute of Technology, Karlsruhe 76131, Germany,
attila.genda@kit.edu,
WWW home page: https://www.itm.kit.edu/dynamik/Mitarbeiter_Genda.php
[2] Technion, Israel Institute of Technology, Haifa, 3200003, Izrael

Abstract. The existence and stability of steady-state averaged solutions for a strongly overdamped particle in a cosine potential are analytically studied when subjected to harmonic excitation. The stability loss of these solutions, which oscillate near the bottom of the potential well, can be viewed as an escape problem. The harmonic balance method is used for the analysis up to the first order, including a constant bias term. When a massless particle is assumed, the steady-state solutions oscillate around either the potential well's minima or maxima. However, taking the particle's mass into account alters the structure of the steady-state solution. Within certain excitation parameter ranges, a new set of equilibrium positions for the oscillation center arises, linking the equilibria at the potential's extremities. Interestingly, modulating only the force amplitude can continuously bias the steady-state oscillation center.

Keywords: particle positioning, potential well, overdamped system, harmonic balance, stability analysis

1 Introduction

The precise and efficient control of particles at the microscale to nanoscale remains an area of significant interest, primarily because of its potential applications in fields like rapid prototyping and biomedicine. Traditionally, methods based on optical manipulation were common. However, recent trends show an inclination towards the use of sound fields, which exert acoustic forces for assembly, presenting a direct approach without requiring chemical additives such as photoinitiators. Although the acoustic assembly of particles demonstrates potential in rapid prototyping [1] and cell culture applications [2], its capabilities have been limited mainly to 2D assemblies near boundaries [3, 4] or point-focused tweezing in both air [5, 6] and aquatic settings [7, 8]. Using standing waves to assemble cells or colloidal microparticles often results in highly symmetrical patterns [9, 10, 11]. The closed cavity assembly discussed by *Prisbrey et al.* [12] also has certain geometric challenges.

Recent research by *Melde et al.* [13] has introduced the use of compact holographic ultrasound fields. This technique assembles various materials, including solid microparticles and hydrogel beads, without the need for opposing waves or scaffolds, presenting a promising approach for rapid biofabrication. Separately, an earlier foundational study by *Friedrich and Herschbach* [14] detailed the interactions between intense laser radiation and polarizable molecules. Their work highlighted the formation of aligned pendular states, indicating a potential for laser alignment and molecular trapping.

The harmonic balance method is a well-researched technique in the literature. While *Nayfeh and Mook*'s textbook [15] is not solely focused on the harmonic balance, it provides a comprehensive overview of the method, among other topics. The application of the method spans various disciplines, including electrical circuits as described by *Gilbert and Steer* [16, 17], fluid dynamics by *Hall et al.* [18], and mechanical systems discussed by *Sarrouy and Sinou* [19]. Alongside these, *Krack and Gross*'s *Harmonic Balance for Nonlinear Vibration Problems* [20] offers a comprehensive overview of the harmonic balance method in the context of nonlinear vibration problems.

In our study, we examine the positioning of a strongly damped particle in a cosine potential subjected to a harmonic force (cf. Fig. 1), drawing parallels to the behavior of a strongly damped driven pendulum. This research seeks to enhance our understanding of the system's dynamics, with the harmonic balance method employed to describe the system's motion analytically.

The paper is organized as follows. Section 2 introduces the problem formulation. Section 3 employs the harmonic balance method, encompassing zeroth-order and first-order harmonics. Section 4 validates analytic solutions against numerical simulations. Section 5 discusses the broader implications of the results and outlines the limitations of the study. Section 6 summarizes the findings and suggests areas for future research.

2 Problem setting

We investigate the dynamics of a strongly damped particle in a cosine potential under harmonic excitation, as described by Eq. (1). The system is mechanically analogous to a damped pendulum in a gravitational field subject to periodic external momentum, as depicted in Fig. 2. The governing equation of motion is expressed as:

$$m\ddot{x} + k\dot{x} + c\sin x = f\sin(\omega\tau + \beta), \tag{1}$$

where:

- m is the mass parameter without further assumptions on its magnitude.
- k is a large damping coefficient that ensures an overdamped regime such that $k = \mathcal{O}(1)$.
- $c\sin x$ represents the restoring force of the potential.
- f denotes the amplitude of the external forcing and is also of the order $\mathcal{O}(1)$.

No specific conditions are imposed on the excitation frequency, ω, and the initial phase, β.

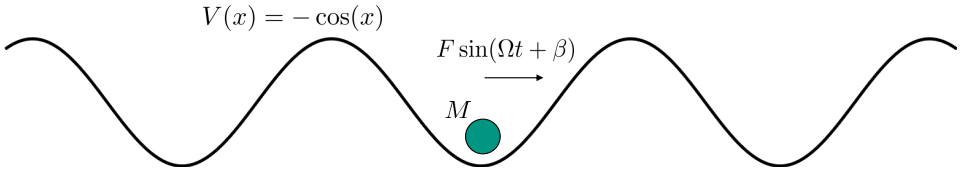

Fig. 1: Problem setting

We introduce a coordinate transformation $\tau = \omega_0 t$ to further analyze the system, which leads to the following differential relations:

$$\omega_0 \square' := \omega_0 \frac{\mathrm{d}\square}{\mathrm{d}t} = \frac{\mathrm{d}}{\mathrm{d}\tau}, \qquad \omega_0^2 \frac{\mathrm{d}^2}{\mathrm{d}t^2} = \frac{\mathrm{d}^2}{\mathrm{d}\tau^2}. \tag{2}$$

Upon application of the transformation, Eq. (1) can be recast in the following form:

$$\frac{\omega_0 m}{k} x'' + x' + \frac{c}{k\omega_0} \sin x = \frac{f}{k\omega_0} \sin\left(\frac{\omega}{\omega_0} t + \beta\right). \tag{3}$$

By setting the frequency as $\omega_0 := c/k$ and introducing the dimensionless frequency $\Omega := k\omega/c$, the equation becomes as follows:

$$\frac{cm}{k^2} x'' + x' + \sin x = \frac{f}{k\omega_0} \sin(\Omega t + \beta). \tag{4}$$

Consequently, the system's dimensionless mass and force parameters are defined by

$$M := \frac{cm}{k^2}, \qquad F := \frac{f}{k\omega_0}, \tag{5}$$

yielding the nonlinear differential equation

$$Mx'' + x' + \sin x = F \sin(\Omega t + \beta). \tag{6}$$

Numerical simulations suggest that the steady-state solutions of this system are not limited to being centered at the bottom of the potential, as depicted in Fig. 3a. The solutions can also be centered around the top, given certain values of F, as illustrated in Fig. 3c.

Furthermore, solutions placed between these two points are also feasible, as highlighted in Fig. 3b. Hence, the symmetry breaking bias can be observed in stationary solutions, which we will capture analytically in the next section.

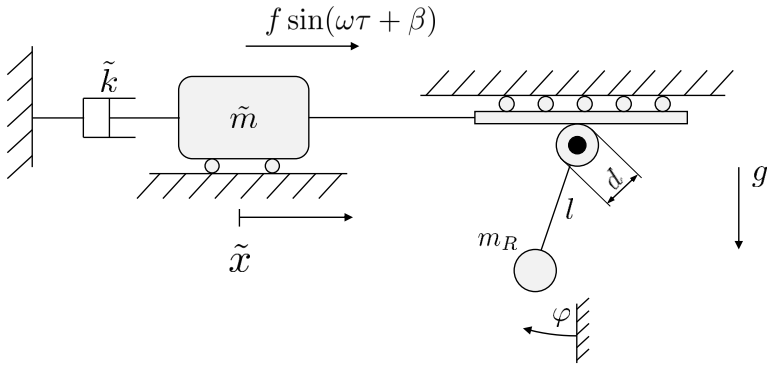

Fig. 2: Analogous mechanical model of the problem. Eq. (1) is obtained by setting $m = \frac{\tilde{m}d}{2} + \frac{2m_R l^2}{d}$, $k = \frac{\tilde{k}d}{2}$, $c = \frac{2m_R g l}{d}$ and $x \equiv \varphi = \frac{\tilde{x}d}{2}$

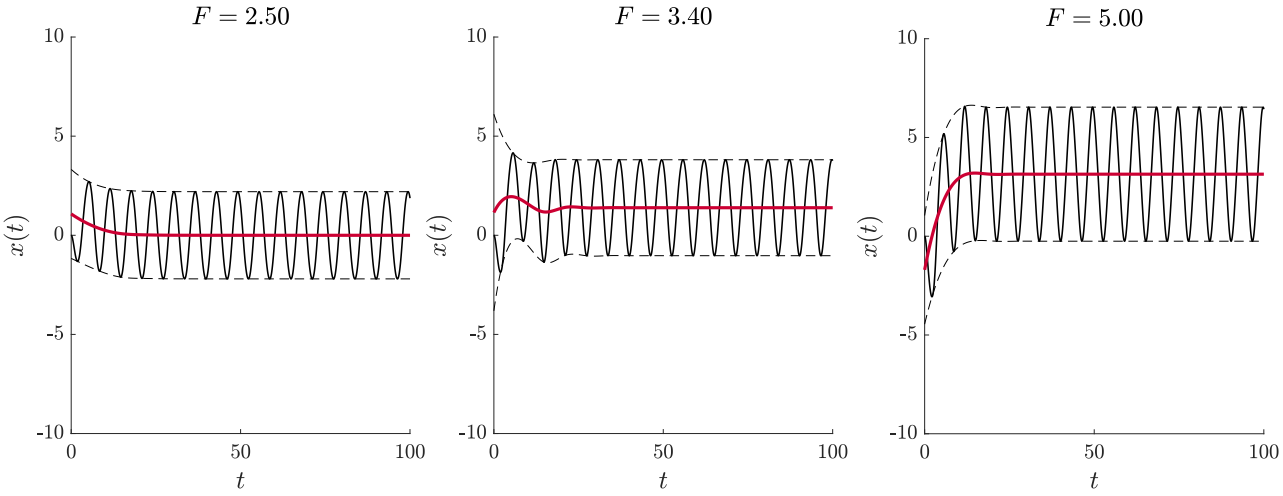

(a) Bottom (b) Intermediate (c) Top

Fig. 3: Different kinds of solutions (black continuous curves) for parameter values $M = 1$, $\Omega = 1$, $\beta = \pi/2$ with homogeneous initial conditions. The center of the vibration (red curve) can be stable at the bottom, top, or any point of the cosine potential, depending on the chosen value of F. In these figures, the center of vibrations is estimated by the mean value of the upper and lower envelopes (dashed black lines) obtained by MATLAB's `envelope` function applied to the numerical simulation data

3 Analytic treatment

In the following section, our analysis will concentrate on determining the steady-state solutions of Eq. (6) and evaluating their stability.

3.1 Harmonic balance

Due to the strong damping, transient solutions decay quickly and only periodic solutions are observed at the steady state. This makes the harmonic balance method suitable for capturing the primary dynamics of the system. To be able to address asymmetric solutions as well, we include a constant (bias) term besides the first harmonic term

$$x_0(t) = A_0 + A_1 \sin(\Omega t + \beta - \Psi). \tag{7}$$

Plugging this into the differential equation, given by Eq. (4), we get:

$$\begin{aligned} M(-\Omega^2 A_1 \sin(\Omega t + \beta - \Psi)) + A_1 \Omega \cos(\Omega t + \beta - \Psi) \\ + \sin(A_0 + A_1 \sin(\Omega t + \beta - \Psi)) = F \sin(\Omega t + \beta). \end{aligned} \tag{8}$$

The last term on the left-hand side of Eq. (8) needs further treatment since a sine function is nested in itself. The Jacobi-Anger expansion, as given by Eqs. (9-10), is suitable for solving this issue.

$$\sin(z\sin(\theta)) = 2\sum_{n=1}^{\infty} J_{2n-1}(z)\sin\left[(2n-1)\theta\right], \tag{9}$$

$$\cos(z\sin(\theta)) = J_0(z) + 2\sum_{n=1}^{\infty} J_{2n}(z)\cos(2n\theta), \tag{10}$$

where $J_n(z)$ is the Bessel function of the first kind of order n.
Applying Eqs. (9-10) to Eq. (8), we can derive three nonlinear algebraic equations by grouping the constant, the $\sin(\Omega t + \beta)$, and the $\cos(\Omega t + \beta)$ terms:

$$J_0(A_1)\sin A_0 = 0, \tag{11}$$

$$-A_1\Omega^2 M\cos\Psi + A_1\Omega\sin\Psi + 2\cos A_0 J_1(A_1)\cos\Psi = F, \tag{12}$$

$$A_1\Omega^2 M\sin\Psi + A_1\Omega\cos\Psi - 2\cos A_0 J_1(A_1)\sin\Psi = 0. \tag{13}$$

Eq. (11) has three different kinds of solutions, corresponding to solution families (SF): A_0 is either located at the bottom (bottom SF) or the top (top SF) of the cosine potential; or the value of A_1 is a root of the Bessel function J_0 (intermediate SF), i.e.,

$$A_{0,1} = 2k\pi, \qquad k \in \mathbf{Z}, \tag{14}$$

$$A_{0,2} = (2k+1)\pi, \qquad k \in \mathbf{Z}, \tag{15}$$

$$A_{1,3} = J_0^{-1}(0), \qquad A_{1,3} > 0, \tag{16}$$

where we define $J_0^{-1}(0)$ as a set-valued expression to denote all positive roots of the Bessel function of the first kind of zeroth order. For the solutions given by Eqs. (14-15), the values of A_1 and Ψ still have to be determined from Eqs. (12-13), whereas in case of Eq. (16) the value of A_0 and Ψ must be determined using the remaining equations (12-13).

The following three SBs are given.

Bottom SF Inserting Eq. (14) in Eqs. (12-13) and applying some algebra, we can separate Ψ and A_1 in two distinct equations

$$\sin\Psi_1 = \frac{A_{1,1}\Omega}{F}, \tag{17}$$

$$\left(A_{1,1}\Omega^2 M - 2J_1(A_{1,1})\right)^2 + A_{1,1}^2\Omega^2 = F^2. \tag{18}$$

Eq. (18) cannot be solved explicitly for $A_{1,1}$; however, an asymptotic solution can be given for large values of F when the force exerted by the cosine potential becomes negligible compared to the damping and inertial forces

$$A_{1,1} \approx \frac{F}{\Omega}\frac{1}{\sqrt{\Omega^2 M^2 + 1}}, \quad \text{for } F \gg 1. \tag{19}$$

Top SF Similarly, by inserting Eq. (15) in Eqs. (12-13) and performing the same algebraic steps, we can separate Ψ and A_1:

$$\sin\Psi_2 = \frac{A_{1,2}\Omega}{F}, \tag{20}$$

$$\left(A_{1,2}\Omega^2 M + 2J_1(A_{1,2})\right)^2 + A_{1,2}^2\Omega^2 = F^2, \tag{21}$$

thus, the equations for the top SF and the bottom SF only differ in the sign of $2J_1(A_{1,2})$.

Intermediate SF The derivation of this family of solutions differs from the previous ones since the possible values of A_1 are already known; instead, A_0 is sought. Let us denote the k^{th} root of $J_0(A_1)$ by α_k. Using this notation, we can rewrite Eqs. (12-13) as

$$\left(2\cos A_0 J_1(\alpha_k) - \alpha_k\Omega^2 M\right)\cos\Psi + \alpha_k\Omega\sin\Psi = F, \tag{22}$$

$$-\left(2\cos A_0 J_1(\alpha_k) - \alpha_k\Omega^2 M\right)\sin\Psi + \alpha_k\Omega\cos\Psi = 0, \tag{23}$$

from which follows that

$$\sin\Psi_3 = \frac{\alpha_k\Omega}{F}, \tag{24}$$

$$\left(2\cos A_0 J_1(\alpha_k) - \alpha_k\Omega^2 M\right)^2 + \alpha_k^2\Omega^2 = F^2. \tag{25}$$

Eq. (25) can be resolved for the bias term as

$$A_0 = 2\pi l \pm \arccos\left(\frac{\alpha_k\Omega^2 M \pm \sqrt{F^2 - \alpha_k^2\Omega^2}}{2J_1(\alpha_k)}\right), \quad l \in \mathbf{Z}. \tag{26}$$

On the contrary to the bottom and top SFs, the intermediate SF does not always exist. The solution exists if the arccos function has real arguments on $[-1, 1]$. To secure a real argument,

$$\alpha_k\Omega < F \tag{27}$$

has to be fulfilled. Furthermore, the arccos function will take real values if the inequalities

$$-1 \le \frac{\alpha_k\Omega^2 M \pm \sqrt{F^2 - \alpha_k^2\Omega^2}}{2J_1(\alpha_k)} \le 1 \tag{28}$$

are fulfilled. If $J_1(\alpha_k) > 0$ then we have

$$-2J_1(\alpha_k) - \alpha_k\Omega^2 M \le \quad \pm\sqrt{F^2 - \alpha_k^2\Omega^2} \quad \le 2J_1(\alpha_k) - \alpha_k\Omega^2 M, \tag{29}$$

otherwise, we have

$$-2J_1(\alpha_k) - \alpha_k\Omega^2 M \ge \quad \pm\sqrt{F^2 - \alpha_k^2\Omega^2} \quad \ge 2J_1(\alpha_k) - \alpha_k\Omega^2 M. \tag{30}$$

Whether the term with F should be taken with a plus or minus sign can be determined by case distinction. We only investigate the case $J_1(\alpha_k) > 0$, given by Eq. (29), since the procedure and results are analogous for Eq. (30).

The left term of Eq. (29) is always negative, and its right term is negative for

$$\frac{2J_1(\alpha_k)}{\alpha_k\Omega^2} < M, \tag{31}$$

in which case only $-\sqrt{F^2-\alpha_k^2\Omega^2}$ is feasible. Then, we have

$$\sqrt{\left(\alpha_k\Omega^2M-2J_1(\alpha_k)\right)^2+\alpha_k^2\Omega^2} \le F \le \sqrt{\left(\alpha_k\Omega^2M+2J_1(\alpha_k)\right)^2+\alpha_k^2\Omega^2}, \tag{32}$$

that always fulfills inequality (27) as well.

However, if

$$\frac{2J_1(\alpha_k)}{\alpha_k\Omega^2} > M, \tag{33}$$

then case $-\sqrt{F^2-\alpha_k^2\Omega^2}$ always fulfills the right hand side of inequality (29), but also $+\sqrt{F^2-\alpha_k^2\Omega^2}$ does so for

$$\alpha_k\Omega \le F \le \sqrt{\left(2J_1(\alpha_k)-\alpha_k\Omega^2M\right)^2+\alpha_k^2\Omega^2}, \tag{34}$$

thus, in this case, the two kinds of solutions

$$A_0 = 2\pi l \pm \arccos\left(\frac{\alpha_k\Omega^2M\pm\sqrt{F^2-\alpha_k^2\Omega^2}}{2J_1(\alpha_k)}\right), \quad l\in\mathbf{Z}, \tag{35}$$

exist. For

$$\sqrt{\left(\alpha_k\Omega^2M-2J_1(\alpha_k)\right)^2+\alpha_k^2\Omega^2} \le F \le \sqrt{\left(\alpha_k\Omega^2M+2J_1(\alpha_k)\right)^2+\alpha_k^2\Omega^2}, \tag{36}$$

only

$$A_0 = 2\pi l \pm \arccos\left(\frac{\alpha_k\Omega^2M-\sqrt{F^2-\alpha_k^2\Omega^2}}{2J_1(\alpha_k)}\right), \quad l\in\mathbf{Z}, \tag{37}$$

exists.

The existence of two distinct kinds of solution within the intermediate SF in the parameter region given by Eq. (33) is an artifact of our chosen ansatz. In none of the numerical simulations, such double solutions could be observed (cf. Fig. 4a and 5a). In fact, by increasing the values of the amplitude of the force, the center of vibration A_0 shifts continuously and smoothly from the bottom of the potential to the top and vice versa.

As mentioned previously, in the case of $J_1(\alpha_k) < 0$, the calculation is very similar, and the artificial double solution parameter region emerges similarly.

3.2 Stability analysis of the steady-state solutions

The steady-state solutions for Eq. (4) have been identified. However, their stability still needs to be ascertained. We introduce a small perturbation δ in the steady-state solution x_0 as follows:

$$x(t) = x_0(t) + \delta(t), \tag{38}$$

and insert it in Eq. (6) to find

$$M\ddot{x}_0 + M\ddot{\delta} + \dot{x}_0 + \dot{\delta} + \sin(x_0 + \delta) = F\sin(\Omega t + \beta), \tag{39}$$

after linearizing the sine term around x_0, we have

$$M\ddot{x}_0 + M\ddot{\delta} + \dot{x}_0 + \dot{\delta} + \sin(x_0) + \cos(x_0)\delta = F\sin(\Omega t + \beta). \tag{40}$$

Given that x_0 satisfies the differential equation (6) within the first harmonic approximation, we can simplify Eq. (39) by letting the terms cancel each other out. We obtain the following.

$$M\ddot{\delta} + \dot{\delta} + \cos(x_0)\delta = 0. \tag{41}$$

Eq. (41) is a linear differential equation with parametric excitation due to x_0 being a function of time. One way to obtain information on the stability of the solutions would be to determine the Floquet multipliers. However, it is notable that the dynamics of δ is extremely slow when the stability of the solution $\delta(t) = 0$ is lost. Therefore, we can average the "fast" dynamics with frequency Ω after making use of the Jacobi-Anger expansion again. Using Eq. (10), we find the average value

$$\langle\cos(A_0 + A_1\sin(\Omega t - \Psi))\rangle = \tag{42}$$

$$= \langle\cos A_0\cos(A_1\sin(\Omega t - \Psi)) - \sin A_0\sin(A_1\sin(\Omega t - \Psi))\rangle \tag{43}$$

$$= \left\langle \cos A_0 \left(J_0(A_1) + 2\sum_{n=1}^{\infty} J_{2n}(A_1)\cos(2n(\Omega t - \Psi)) \right) \right\rangle$$

$$- \left\langle \sin A_0 \left(2\sum_{n=1}^{\infty} J_{2n-1}(A_1)\sin\left[(2n-1)(\Omega t - \Psi)\right] \right) \right\rangle \tag{44}$$

$$= \cos A_0 J_0(A_1). \tag{45}$$

Hence, the average of Eq. (41) becomes

$$M\ddot{\delta} + \dot{\delta} + \cos A_0 J_0(A_1)\delta = 0. \tag{46}$$

Taking the values of A_0 and A_1 corresponding to the different SBs, we can use a simple linear stability analysis to determine the stability of the steady-state solutions found in Secs. 3.1-3.1. For asymptotic stability, $\cos A_0 J_0(A_1) > 0$ must be fulfilled.

Stability of the bottom SF When the center of vibration, A_0, is at the bottom of the potential well, we have $\cos A_0 = 1$. Thus, the corresponding solution is stable if $J_0(A_1)$ has a positive sign. Since the change of A_1 is continuous in F, two consecutive roots of $J_0(A_1) = 0$ define the stability boundaries. Inserted in Eq. (18), these roots provide the critical forcing values where the stability of the steady-state solution changes:

$$F_{\mathrm{crit},1,k} = \sqrt{\left(2J_1(\alpha_k) - \alpha_k\Omega^2 M\right)^2 + \alpha_k^2\Omega^2}, \tag{47}$$

with α_k being the k^{th} root of $J_0(A_1)$. Hence, the steady-state solution is stable for the following conditions.

$$\sqrt{\left(2J_1(\alpha_{2k}) - \alpha_{2k}\Omega^2 M\right)^2 + \alpha_{2k}^2\Omega^2} < F < \sqrt{\left(2J_1(\alpha_{2k+1}) - \alpha_{2k+1}\Omega^2 M\right)^2 + \alpha_{2k+1}^2\Omega^2}, \tag{48}$$

with $k \in \mathbf{N}$ and $\alpha_0 := 0$.

Stability of the top SF When the center of vibrations is at the top of the potential, the situation is similar to the previous one with the difference that now $\cos A_0 = -1$; thus, the solution at the top of the potential becomes stable for negative values of $J_0(A_1)$. Since A_1 is the solution of Eq. (21), the critical forcing values, where the stability of the steady-state solution changes, are determined by

$$F_{\mathrm{crit},2,k} = \sqrt{\left(2J_1(\alpha_k) + \alpha_k \Omega^2 M\right)^2 + \alpha_k^2 \Omega^2}, \tag{49}$$

with α_k being the k^{th} root of $J_0(A_1)$. Hence, a steady-state solution is stable for

$$\sqrt{\left(2J_1(\alpha_{2k+1}) + \alpha_{2k+1} \Omega^2 M\right)^2 + \alpha_{2k+1}^2 \Omega^2} < F < \sqrt{\left(2J_1(\alpha_{2k+2}) + \alpha_{2k+2} \Omega^2 M\right)^2 + \alpha_{2k+2}^2 \Omega^2}, \tag{50}$$

with $k \in \mathbf{N}$.

We can observe that the parameter regions, defined by Eqs. (48) and (50), are disjoint and do not cover all possible values of F. There are parameter regions of F, where neither the solution with a vibration center at the bottom of the potential nor a vibration center at the top of the potential is stable. This topological argument suggests that some solution in between must be stable.

Stability of the intermediate SF The linear stability analysis does not give any statement regarding the stability of the intermediate SF because the values of A_1 are determined by the roots of $J_0(A_1)$. Consequently, the term $\cos A_0 J_0(A_1)$ invariably equals zero, leading to an eigenvalue in Eq. (46) that has a real part of zero. Due to the problem's linearization, it is impossible to determine stability from this conclusively. However, it is noteworthy that both topological considerations and results from thousands of numerical simulations suggest that the intermediate SF given by Eq. (37) is stable for

$$\sqrt{\left(2J_1(\alpha_{2k+1}) - \alpha_{2k+1} \Omega^2 M\right)^2 + \alpha_{2k+1}^2 \Omega^2} < F < \sqrt{\left(2J_1(\alpha_{2k+1}) + \alpha_{2k+1} \Omega^2 M\right)^2 + \alpha_{2k+1}^2 \Omega^2} \tag{51}$$

and

$$\sqrt{\left(2J_1(\alpha_{2k+2}) + \alpha_{2k+2} \Omega^2 M\right)^2 + \alpha_{2k+2}^2 \Omega^2} < F < \sqrt{\left(2J_1(\alpha_{2k+2}) - \alpha_{2k+2} \Omega^2 M\right)^2 + \alpha_{2k+2}^2 \Omega^2}, \tag{52}$$

with $k \in \mathbf{N}$ and $\alpha_0 := 0$. Note that the sign of $J_1(\alpha_k)$ alternates for consecutive values of k, making Eqs. (51-52) consistent with Eqs. (48) and (50).

4 Validation

In Fig. 4a, we display the numerically derived steady-state center of vibration as a function of parameters F and M. A more detailed view of the parameter region $F = 2.65 \ldots 2.71$ and $M = 0.001 \ldots 0.05$ is provided in Fig. 5a. The analytical estimate for the center of steady-state oscillations is shown in Fig. 4b. There is a clear qualitative agreement between the analytic and numerical results. However, some discrepancies between them can be observed; for example, the first predicted value, where the stability of the steady-state solution changes when $M = 0$, is numerically obtained at $F_{\mathrm{crit,num}}(M = 0) = 2.677$. At the same time, the analytic prediction is $F_{\mathrm{crit,anal}}(M = 0) = 2.619$. Similarly, the transition region from $A_0 = 0$ to $A_0 = \pi$ is offset by some amount for $M \neq 0$.

Enhancing the harmonic balance approach by incorporating even a single additional term, like:

$$x_0(t) = A_0 + A_1 \sin(\Omega t - \Psi_1) + A_2 \sin(2\Omega t - \Psi_2), \tag{53}$$

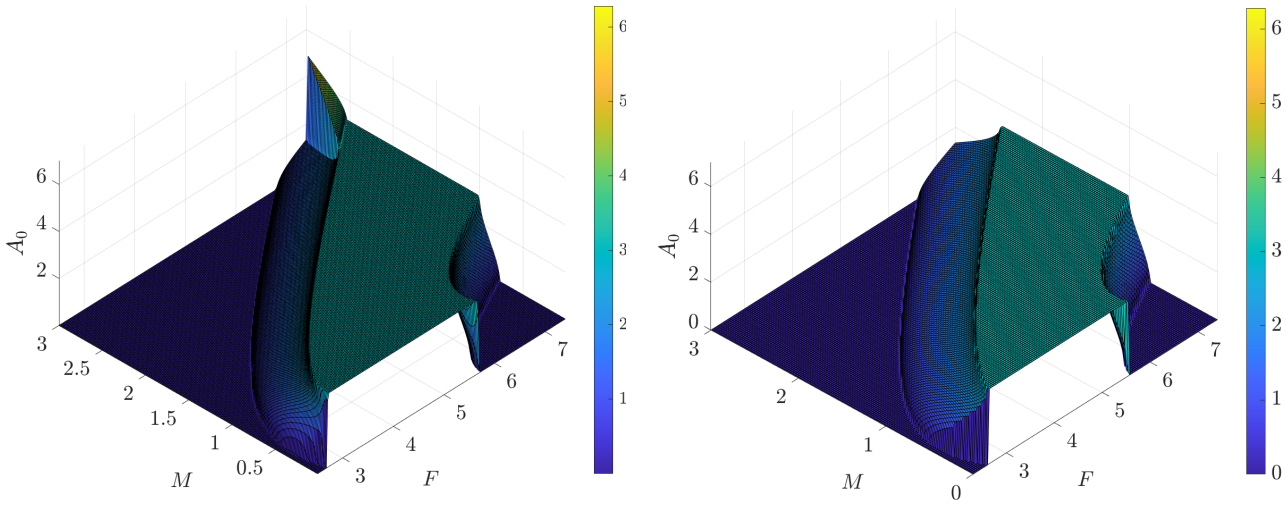

(a) Numerically obtained centers of vibration. Bifurcation in the upper corner due to Eq. (37) prescribing a family of solutions. The actual solution depends on the excitation phase and initial conditions

(b) Analytically obtained centers of vibration. The function in the bottom corner is not displayed correctly due to the artificial double-solution of the harmonic balance ansatz. Simulations show a continuous transition from 0 to π

Fig. 4: Position of the center of steady state vibrations against the values of F and M with $\Omega = 1$, $\beta = \pi/2$ and homogeneous initial conditions

significantly complicates the problem to the point where analytic solutions become nearly unmanageable.

Yet, numerically, we can observe that the intermediate solution breaks the symmetry not only by its biased vibration center but also by its non-vanishing even Fourier terms. To demonstrate this, in Fig. 6, two examples are given, where the Fourier coefficients of the periodic steady-state solution are determined by the numerical evaluation of Eq. (54)

$$C_k = \frac{1}{T} \int_{t_\infty}^{t_\infty + T} x(t) e^{-i\Omega k t} \mathrm{d}t, \tag{54}$$

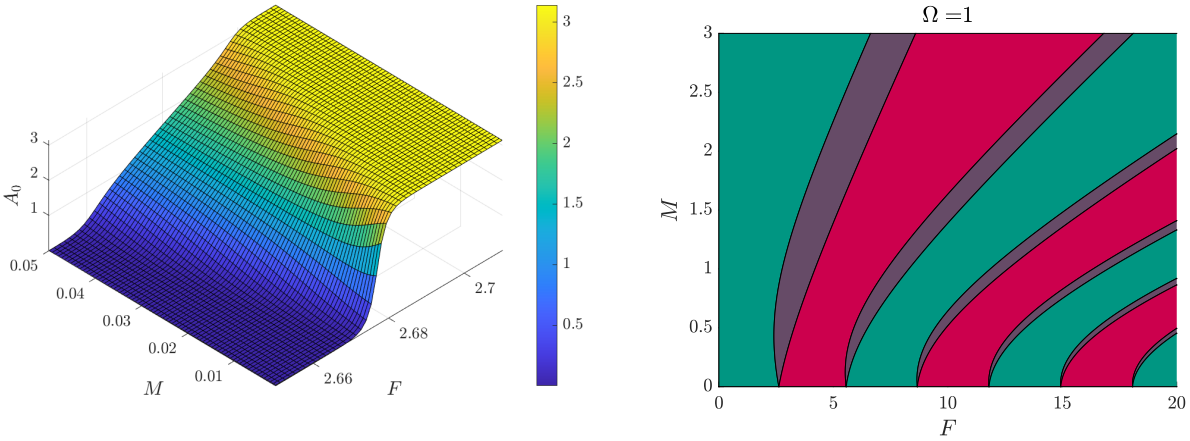

(a) High-resolution view of the bottom corner of Fig. 4a

(b) Stable steady-state solutions

Fig. 5: Comparison of numerical and analytic results against parameters F and M. The left subfigure shows the numerical results for small mass values, while the right presents the analytically obtained stable steady-state solutions: bottom (green), top (red) and intermediate (purple). In the left figure, for $M = 0$, the function converges to a step function at $F_{\text{crit}} = 2.677$ that changes from $A_0 = 0$ to $A_0 = \pi$

where $T = 2\pi/\Omega$; and t_∞ denotes a sufficiently late time instance after which the transient motion might be neglected. With these coefficients, the steady-state solution can be represented as

$$x(t) = \sum_{k=-\infty}^{\infty} C_k e^{i\Omega k t}. \tag{55}$$

5 Discussion

This paper investigated steady-state solutions of an overdamped particle in a cosine potential under harmonic excitation. Depending on the particle's mass, the exciting force amplitude, and the excitation frequency, the center of the steady-state oscillation might differ. One can observe that by increasing the value of F, at a certain level, the center of vibration starts to shift continuously from the bottom position $2k\pi$ to the neighboring top position $(2k \pm 1)\pi$, where after reaching a certain critical force level, the center of oscillation settles. After the excitation force is further increased, a continuous shift of the center of oscillation starts back to the bottom position. This process repeats itself infinitely, although the transition from the bottom to the top of the potential always happens faster by increasing the values of F. The observed continuous shift is an effect of the particle's mass; in the case of a massless particle, the continuous shift cannot be observed; it is reduced to a discontinuous jump in the value of the center of steady vibrations.

Furthermore, the initial conditions and the starting phase of the excitation have a minor impact on the steady-state outcome of the system. They determine the location of the vibration center but do not change the stable solution family itself, as shown in Fig. 4a.

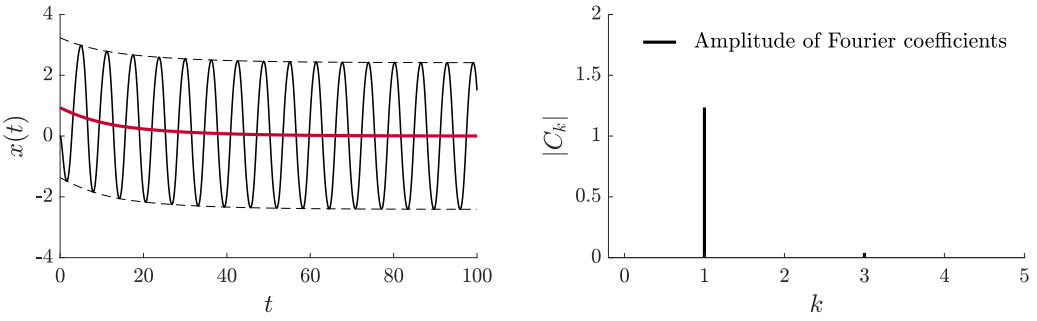

(a) Symmetric steady-state solution with $F = 2.5$

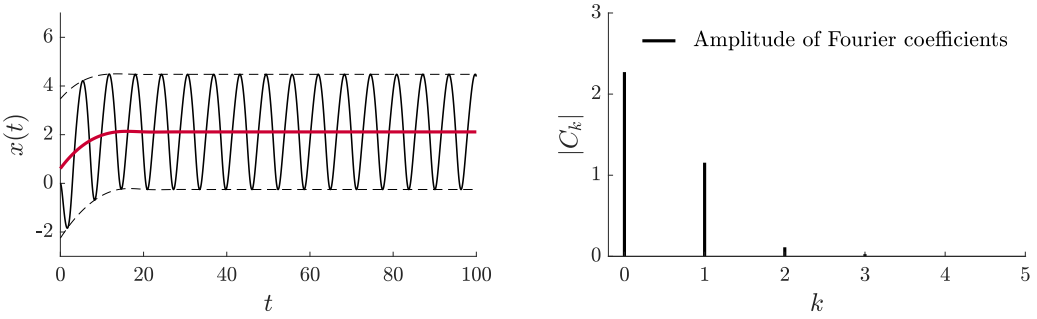

(b) Asymmetric steady-state solution with $F = 3$

Fig. 6: Solution $x(t)$ decaying to steady state (on the left) and the amplitudes of its spectral decomposition $|C_k|$ (on the right) with parameter values $M = 0.5$, $F = \{2.5, 3\}$, $\Omega = 1$ and $\beta = -\pi/2$ using homogeneous ICs. The red line denotes the center of vibration, while the dashed line is the vibration envelope

At first glance, it seems that the mass of the particle is responsible for the surprising asymmetric dynamics of the system. However, we should realize that the system dynamics is naturally asymmetrical, and neglecting the mass results in degenerate symmetric dynamics, as revealed by Eqs. (12-13). A rather intuitive explanation for what has been derived analytically in the paper is as follows.

For a given excitation, the resulting steady-state vibration amplitude is largely determined by the damping and, eventually, by the mass of the particle. However, the underlying force of the potential also contributes to the steady-state amplitude value. This contribution is based on the average force acting on the particle during one period of its supposed steady-state movement. Depending on the magnitude of the exciting force, the potential's average force can either increase or decrease the amplitude of the steady-state solution compared to the case of a damped free particle (without potential). In most cases, this will either result in a bottom- or top-stabilized vibration center. However, for the same excitation, the steady-state vibration amplitude at the bottom is always different from the top one. Thus, when the steady-state solution loses its stability around one of the positions, the other one still has not gained stability. Therefore, if there is any stable periodic solution in such a case, it must be centered at an intermediate position between the bottom and the top of the potential.

In contrast, when a massless particle is considered, the structure of the system degenerates: it becomes a first-order system, and as such, it is no "classical" mechanical system anymore. Thus, our intuition, accustomed to second-order mechanical systems, is deceived. In the model reduction with no mass, may it only be an artifact, the steady-state vibration amplitude at the top and at the bottom are equal. Thus, by the loss of stability at one of them, stability is immediately gained at the other.

6 Conclusions and scope for future research

The existence of a stable biased steady-state solution in what appears to be a symmetric problem raises a crucial question in research methodology: the selection of an appropriate ansatz. This finding underscores the need for an initial (often numerical) exploration phase preceding analytical treatment. Properly executed, this exploratory phase enables researchers to identify key system parameters and anticipate the types of bifurcations that may occur. Although experienced researchers might accurately predict system behavior through intuitive thought experiments, even straightforward scenarios like the one detailed in this paper can yield surprising dynamics that risk leading to an incorrect choice of ansatz.

The existence of stable steady-state solutions with an intermediate center of vibration has practical implications as well. The overdamped particle M might be a molecule actuated by an electromagnetic or acoustic field. Its position might be controlled only by changing the value of the excitation amplitude, and there is no need to control the excitation phase.

These results have potential applications in ultrasound-driven particle systems and in the design of microelectromechanical systems.

A pressing question from this study is about the nature of potentials that allow the vibration center to shift continuously just by increasing the excitation force's amplitude. Identifying the conditions for such potentials remains a valuable area for further research.

Acknowledgment

This work was funded by the Deutsche Forschungsgemeinschaft (DFG, German Research Foundation) - Project number: 508244284. This support is greatly appreciated.

Data availability

This manuscript does not have associated data.

Declarations

The authors have nothing to declare.

Conflict of interest

The authors declare that they have no conflict of interest.

Bibliography

[1] K. Melde, E. Choi, Z. Wu, S. Palagi, T. Qiu, and P. Fischer. Acoustic fabrication via the assembly and fusion of particles. *Adv. Mater.*, 30:1704507, 2018.

[2] Z. Ma, A.W. Holle, K. Melde, T. Qiu, K. Poeppel, V.M. Kadiri, and P. Fischer. Acoustic holographic cell patterning in a biocompatible hydrogel. *Adv. Mater.*, 32:1904181, 2020.

[3] K. Melde, A.G. Mark, T. Qiu, and P. Fischer. Holograms for acoustics. *Nature*, 537:518–522, 2016.

[4] Y. Gu, C. Chen, J. Rufo, C. Shen, Z. Wang, P.H. Huang, H. Fu, P. Zhang, S.A. Cummer, Z. Tian, and T.J. Huang. Acoustofluidic holography for micro- to nanoscale particle manipulation. *ACS Nano*, 14:14635–14645, 2020.

[5] A. Marzo, S. A. Seah, B. W. Drinkwater, D. R. Sahoo, B. Long, and S. Subramanian. Holographic acoustic elements for manipulation of levitated objects. *Nature Communications*, 6:8661, 2015.

[6] A. Marzo and B. W. Drinkwater. Holographic acoustic tweezers. *Proceedings of the National Academy of Sciences*, 116(1):84–89, 2019.

[7] D. Baresch, J. L. Thomas, and R. Marchiano. Observation of a single-beam gradient force acoustical trap for elastic particles: Acoustical tweezers. *Phys. Rev. Lett.*, 116:024301, 2016.

[8] A. Franklin, A. Marzo, R. Malkin, and B. W. Drinkwater. Three-dimensional ultrasonic trapping of micro-particles in water with a simple and compact two-element transducer. *Applied Physics Letters*, 111(9):094101, 2017.

[9] J. P. K. Armstrong, J. L. Puetzer, A. Serio, A. G. Guex, M. Kapnisi, A. Breant, Y. Zong, V. Assal, S. C. Skaalure, O. King, T. Murty, C. Meinert, A. C. Franklin, P. G. Bassindale, M. K. Nichols, C. M. Terracciano, D. W. Hutmacher, B. W. Drinkwater, T. J. Klein, A. W. Perriman, and M. M. Stevens. Engineering anisotropic muscle tissue using acoustic cell patterning. *Adv. Mater.*, 30:e1802649, 2018.

[10] J. P. K. Armstrong, E. Pchelintseva, S. Treumuth, C. Campanella, C. Meinert, T. J. Klein, D. W. Hutmacher, B. W. Drinkwater, and M. M. Stevens. Tissue engineering cartilage with deep zone cytoarchitecture by high-resolution acoustic cell patterning. *Adv. Healthc. Mater.*, page e2200481, 2022.

[11] M. Caleap and B. W. Drinkwater. Acoustically trapped colloidal crystals that are reconfigurable in real time. *Proc. Natl. Acad. Sci. U.S.A.*, 111:6226–6230, 2014.

[12] M. Prisbrey, J. Greenhall, F. G. Vasquez, and B. Raeymaekers. Ultrasound directed self-assembly of three-dimensional user-specified patterns of particles in a fluid medium. *J. Appl. Phys.*, 121:014302, 2017.

[13] Kai Melde, Heiner Kremer, Minghui Shi, Senne Seneca, Christoph Frey, Ilia Platzman, Christian Degel, Daniel Schmitt, Bernhard Schölkopf, and Peer Fischer. Compact holographic sound fields enable rapid one-step assembly of matter in 3d. *Science Advances*, 9(6):eadf6182, 2023.

[14] Bretislav Friedrich and Dudley Herschbach. Alignment and trapping of molecules in intense laser fields. *Phys. Rev. Lett.*, 74:4623–4626, Jun 1995.

[15] A.H. Nayfeh and D.T. Mook. *Nonlinear Oscillations*, volume 1979. Wiley, New York, 1979.

[16] R.J. Gilmore and M.B. Steer. Nonlinear circuit analysis using the method of harmonic balance—a review of the art. part i. introductory concepts. *Int. J. Microw. Millimeter-Wave Comput. Aided Eng.*, 1(1):22–37, 1991.

[17] R.J. Gilmore and M.B. Steer. Nonlinear circuit analysis using the method of harmonic balance—a review of the art. ii. advanced concepts. *Int. J. Microw. Millimeter-Wave Comput. Aided Eng.*, 1(2):159–180, 1991.

[18] K.C. Hall, J.P. Thomas, and W.S. Clark. Computation of unsteady nonlinear flows in cascades using a harmonic balance technique. *AIAA J.*, 40(5):879–886, 2002.

[19] E. Sarrouy and J.J. Sinou. *Non-linear periodic and quasi-periodic vibrations in mechanical systems-on the use of the harmonic balance methods*. Intech, 2011.

[20] Malte Krack and Johann Gross. *Harmonic Balance for Nonlinear Vibration Problems*. Mathematical Engineering. Springer Cham, Cham, 1 edition, 2019. Number of Pages: XII, 159. Number of Illustrations: 21 b/w illustrations, 35 illustrations in colour. Topics: Engineering Mathematics, Solid Mechanics, Fourier Analysis, Multibody Systems and Mechanical Vibrations.